Efficient and Stable Wide Bandgap Perovskite Solar Cells through Surface Passivation with Long Alkyl Chain Organic Cations

The Duong,[1,*] , *Huyen Pham*,[2] *Yanting Yin*,[3,4] *Jun Peng*,[1] *Md Arafat Mahmud*,[1,**] *YiLiang Wu*,[1] *Heping Shen*,[1] *Jianghui Zheng*,[5,6] *Thanh Tran-Phu*,[7] *Teng Lu*,[8] *Li Li*,[9] *Anand Kumar*,[3,4] *Gunther G. Andersson*,[3,4] *Anita Ho-Baillie*,[5,6] *Yun Liu*,[8] *Thomas White*,[1] *Klaus Weber*,[1] *Kylie Catchpole*[1,*]

[1]School of Engineering, The Australian National University, Canberra 2601, Australia

[2]Department of Electronic Materials Engineering, Research School of Physics, The Australian National University, Canberra 2601, Australia

[3]Flinders Institute for Nanoscale Science and Technology, Flinders University, Adelaide, SA 5042, Australia

[4]Flinders Microscopy and Microanalysis, College of Science and Engineering, Flinders University, Adelaide, SA 5042, Australia

[5]The University of Sydney Nano Institute (Sydney Nano) and School of Physics, University of Sydney, Sydney 2006, Australia

[6]Australian Centre for Advanced Photovoltaics (ACAP), School of Photovoltaic and Renewable Energy Engineering, University of New South Wales, Sydney 2052, Australia

[7]Nanotechnology Research Laboratory, School of Engineering, The Australian National University, Canberra 2601, Australia

[8]Research School of Chemistry, The Australian National University, Canberra 2601, Australia

[9]Australian National Fabrication Facility (ANFF), Department of Electronic Materials Engineering, The Australian National University, Canberra 2601, Australia

[*]**Corresponding Authors**: the.duong@anu.edu.au, kylie.catchpole@anu.edu.au

[**]Present address: The University of Sydney Nano Institute (Sydney Nano) and School of Physics, University of Sydney, Sydney 2006, Australia

Abstract:

Defects on perovskite surfaces acting as charge-carrier-traps are a key factor limiting the performance of perovskite solar cells (PSCs). Here we studied the defect passivation effect of three bromide-containing alkylammonium organic cations with increasing alkyl-chain-length: n-butylammonium bromide, n-octylammonium bromide and n-dodecylammonium bromide on a perovskite composition with 1.72eV bandgap. Long-alkyl-chain organic cations were found to have a greater passivation effect compared to their shorter counterparts due to greater reduction in surface defects and substantial changes in the electronic structure of the passivated perovskite films. The efficiency of 1.72eV PSCs was improved to 19.1% with an excellent open-circuit-voltage of over 1280mV. The long-alkyl-chain passivation significantly improved the moisture and light stability of PSCs as the unencapsulated devices retained >90% of the initial performance after 144h at 70%-85% relative-humidity and >93% of the initial performance after operating under light for 80h. The study has paved the way for efficient and stable wide bandgap perovskite top cells used in perovskite-silicon tandem solar cells.

Keywords: solar cell; perovskite; perovskite-silicon tandem; surface passivation; stability; alkylammonium organic cations

Introduction

Perovskite solar cells have reached a milestone over 25% efficiency after just over a decade of research and development.[1] To commercialize this technology, one of the most promising strategies is to combine perovskite cells with the existing silicon solar cells in tandem configurations. In a two-terminal monolithic perovskite-silicon tandem configuration, a highest efficiency of 29.52% has recently been achieved.[1, 2] While the efficiency of four-terminal

mechanically stacked perovskite-silicon tandem solar cell has slightly lagged behind with the best reported efficiency of 28.3%,[3] both those efficiencies of perovskite-silicon tandem solar cells have significantly surpassed the record efficiency 26.6% of single junction silicon cells. To improve the efficiency of perovskite-silicon tandem solar cells to 30% and beyond, many groups have been focusing on optimizing the perovskite top cells eg. bandgap tuning of the perovskite materials, enhancing the perovskite bulk quality, passivating perovskite surface defects, and engineering the interfaces within the devices. A perovskite bandgap close to 1.7 eV is optimal for perovskite-silicon tandem solar cell efficiency, allowing for a current matching between the perovskite top cell and the silicon bottom cell. This optimal bandgap has been mainly obtained by using mixed-halide anions of iodide and bromide in the perovskite composition.[4-8] For passivating the perovskite surface, many classes of materials have been demonstrated with high performance. Bulky organic cations are known to form two-dimensional (2D) perovskite and have demonstrated great success in passivating the perovskite surface. Cho *et al.* used bulky organic cation iso-butylammonium iodide to passivate the surface of 1.62 eV perovskites and enhanced the efficiency to 21.7%.[9] Using phenethylammonium iodide (PEAI), Jiang *et al.* improved the efficiency of 1.53 eV perovskite to 23.3% and an open circuit voltage (V_{OC}) of 1180 mV.[10] Recently, Kim *et al.* used a series of alkylammonium iodide cations and demonstrated an efficiency of 22.9% in a perovskite solar cell with a low bandgap of 1.52 eV.[11] For perovskites with large bandgap (over 1.7 eV), it has been shown that the bromide containing organic cations work better than their iodide counterparts.[12, 13] For large bandgap perovskites, so far only an alkylammonium cation with a short alkyl chain such as n-butylammonium bromide ($C_4H_{12}NBr$) has been used. Although this has resulted in significantly enhanced perovskite cell performance, the stability of perovskite cells especially in ambient with the presence of moisture was hardly improved due to the poor hydrophobicity of the short alkyl chain materials.[14] In this work, we studied the

effect of passivating large bandgap (1.72 eV) perovskite with a series of bromide containing bulky organic cations with varying alkylammonium chain lengths: n-butylammonium bromide ($C_4H_{12}NBr$, abbreviated as n-BABr), n-octylammonium bromide ($C_8H_{20}NBr$, abbreviated as n-OABr) and n-dodecylammonium bromide ($C_{12}H_{28}NBr$, abbreviated as n-DABr) on the optoelectronic properties of the perovskite films, perovskite solar cell performance and moisture stability. Using sophisticated techniques, we clearly identified the formation of different phases at the perovskite surface upon passivation. These include an ultrathin unreacted alkylammonium organic cation as the topmost layer and a thin pure two-dimensional (2D) perovskite intermixed with the three-dimensional (3D) perovskite underneath. The ultrathin unreacted alkylammonium organic cation was not detected in previous reports [15-17], which is probably due to the limitation in the resolution of the measurements used. We demonstrated that the bromide containing alkylammonium organic cations with long alkyl chain lengths, n-OABr and n-DABr, have much better passivation property compared to the short alkyl chain n-BABr, resulting in greater cell performance. The improvement came from better hole extraction due to reduction in perovskite surface defects and more favorable built-in electric field inside the device as shown by various characterization techniques including photoluminescence (PL) and electron beam induced current (EBIC) measurements. A champion efficiency of 19.1% has been achieved for 1.72 eV bandgap perovskite solar cells with a V_{OC} of 1280 mV. Using n-OABr, the moisture stability of perovskite solar cells was significantly improved, retaining over 90% of the initial efficiency after exposure to 70% – 85% RH for 144 hours. The enhancement in the moisture stability of the n-OABr passivated perovskite cells is likely to be due to the presence of the ultrathin n-OABr layer at the top perovskite surface. The light stability of perovskite cells was also enhanced upon passivation with long alkyl chain organic cations and the n-OABr passivated device retained 93% of the initial efficiency after 80 hours operating under continuous illumination. Overall, passivating

the wide bandgap perovskites with the bromide containing long alkyl chain organic cations (n-OABr and n-DABr) substantially reduces the surface defects, improves the hole extraction efficiency, and leads to greater solar cell performance as well as stability.

Results and discussion

Effect of Passivation on the Performance of 1.72 eV Bandgap Perovskite Solar Cells

We first examined the effect of using different alkylammonium bromide organic cations with varying alkyl chain lengths including n-BABr, n-OABr and n-DABr as a passivation layer on the perovskite surface on the performance of perovskite solar cells. We used the standard perovskite cell structure of glass/ tin doped indium oxide (ITO)/ compact-TiO2/ mesoporous-TiO2/ perovskite/ passivation layer/ Spiro-MeOTAD/ Au as illustrated in **Figure 1a**. The perovskite composition used in this work is $FA_{0.75}MA_{0.15}Cs_{0.1}Rb_{0.05}PbI_2Br$ with a bandgap of 1.72 eV as described in previous reports (**Figure S1**).[8, 12] Here FA and MA stand for formamidinium and methylammonium, respectively. As shown in **Figure 1b** and summarized in **Table S1**, V_{OC} was greatly enhanced from an average of ~1230 mV to ~1260 mV upon passivation with a short alkyl chain n-BABr and the V_{OC} was further increased to ~1270 mV upon passivation with longer alkyl chain organic cations n-OABr and n-DABr. While the short circuit current density (J_{SC}) was almost unchanged, the average fill factor (FF) of the devices was increased from ~72% in control devices to ~76% in n-BABr passivated devices and ~77% in n-OABr and n-DABr passivated devices. As a result, the average efficiency of perovskite solar cells was significantly boosted from ~16.9 ± 0.4% in control devices to ~17.9 ± 0.3% in n-BABr passivated cells and to ~18.4 ± 0.3% in n-OABr and n-DABr passivated devices. Although the n-OABr and n-DABr passivated devices offered similar average efficiencies, the n-OABr passivated devices resulted in the champion efficiency of 19.1% and a V_{OC} over 1280 mV (**Figure S2,3**). This champion efficiency was among the highest efficiencies ever reported for wide bandgap (between 1.7 eV to 1.8 eV) perovskite solar cells (**Table S2**). It is worth

noting that there was a small but notable difference between the efficiencies obtained from the reverse scan and forward scan in the control devices. This hysteresis was almost eliminated upon passivation using any of the three alkylammonium organic cations.

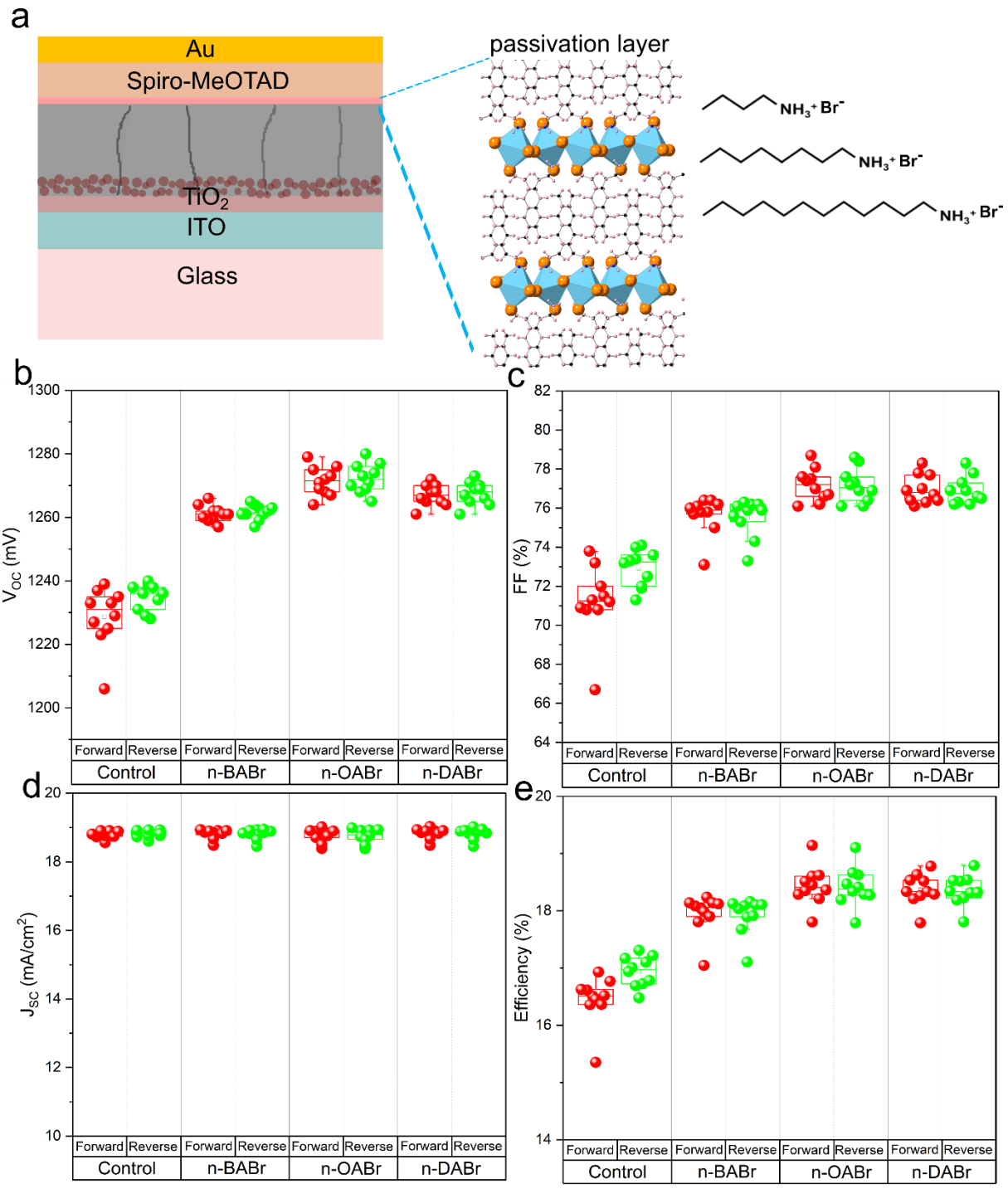

Figure 1. Perovskite solar cell structure and photovoltaic performance. **a** – Schematic of alkylammonium bromide surface passivated perovskite solar cells demonstrated in this work,

b - open circuit voltage (V_{OC}), **c** - fill factor (FF), **d** - short circuit current density (J_{SC}) and **e** - efficiency of perovskite solar cells treated with different alkylammonium bromide cations. Ten devices were tested in each condition.

Effect of Passivation on the Perovskite Surface Elemental Composition and Phase Formation

We next investigated the changes in the morphology of perovskite films upon passivation with different alkylammonium organic cations. As shown in **Figure S4**, the scanning electron microcopy (SEM) images of the perovskite surfaces show negligible change of the film morphology and the three dimensional (3D) perovskite crystal feastures characteristic of the bulk. Atomic Force Microscopy (AFM) images show that the surface roughness of perovskite was slightly reduced from 14.3 nm in control film to between 11 – 12 nm in passivated perovskite films (**Figure S5**). We measured the X-ray photoelectron spectra (XPS) to understand how the surface passivation with different alkylammonium organic cations modified the elemental composition at the perovskite surface. As shown in **Figure 2a,** the C 1s spectra of the control film can be fitted with three individual peaks at 285.2 ± 0.15 eV, 286.4 ± 0.15 eV and 288.6 ± 0.15 eV. The peak at 285.2 ± 0.15 eV (red curve) was attributed to adventitious carbon while the peaks at 286.4 ± 0.15 eV (blue curve) and 288.6 ± 0.15 eV (green curve) were attributed to carbon from the FA and MA cations in the 3D perovskite.[18] Upon passivation with the short alkyl chain n-BABr, the intensity of the peak at 285.2 ± 0.15 eV slightly increased while the intensities at the other peaks slightly decreased. When longer alkyl chain organic cations were used, the intensity of the peak at 285.2 ± 0.15 eV was further enhanced while the intensities of the other peaks at 286.4 ± 0.15 eV and 288.6 ± 0.15 eV were significantly reduced. The increase in the peak intensity at 285.2 ± 0.15 eV originates from the formation of the 2D layer on the perovskite surface since the hydrocarbon (-CH_2-) in the alkylammonium cations has a similar binding energy at 285.2 ± 0.15 eV.[19] This explains the

more significant changes in the C 1s spectrum observed upon passivation with long alkyl chain organic cations (with more hydrocarbon chains) compared to the case with short alkyl chain cation. The finding was verified by fitting the N 1s spectra with two individual peaks at 400.9 ± 0.15 eV and 402.5 ± 0.15 eV, which were assigned to C-N and C-N^+, respectively.[20, 21] Evidently, the peak intensity at 400.9 ± 0.15 eV was reduced while the peak intensity at 402.5 ± 0.15 eV was enhanced due to the formation of the 2D layer (**Figure 2b**). In contrast to the changes in C 1s and N 1s spectra, the spectral changes in Pb 4f, I 3d and Br 3d are less prominent. While the difference in those spectra in the control sample and the n-BABr passivated sample was negligible, we detected small peak shifts (less than 100 meV) in Pb 4f 5/2 and I 3d 3/2 and slightly larger peak shifts (between 100 meV to 200 meV) in Br 3d 5/2 (**Figure S6**) for n-OABr and n-DABr passivated samples. The XPS results indicate that long alkyl chain materials (n-OABr and n-DABr) greatly modify the surface chemistry of 3D perovskite films through the formation of a 2D surface layer, while the modification due to the short chain material (n-BABr) is much weaker.

Grazing incidence X-ray diffraction (GIXRD) measurements were then performed to detect different phases at the film surface. **Figures 2c,d** show additional low angle peaks from the passivated films: $2\theta = 4.35^o$, 8.70^o, $13.05^o$for n-BABr passivated film, $2\theta = 4.06^o$, 8.12^o, 12.18^o for n-OABr passivated film and $2\theta = 3.46^o$,6.92^o, 10.38^o for n-DABr passivated film. It can be clearly observed that the additional peaks move to lower angles as the alkyl chain length of the passivating material increases. As the interplanar spacing should increase as the alkyl chain gets longer, this finding is in agreement with Bragg's law: $\sin\theta = \frac{k\times\lambda}{2\times d}$ where $k = 1$, $\lambda = 1.54$ Å and d is the interplanar spacing at the diffraction angle θ. To understand the origin of the observed additional peaks in the XRD patterns from the passivated films, we measured the diffraction patterns of the pure alkylammonium organic cation n-OABr (main peak at $2\theta = 3.49^o$), pure 2D perovskite phase $(n\text{-}OA)_2Pb(I_{0.67}Br_{0.33})_4$ (main peak at

$2\theta = 4.14^{o}$) and quasi-2D Ruddlesden Popper perovskite phase $(n\text{-}OA)_2A_{n-1}Pb_n(I_{0.67}Br_{0.33})_{3n+1}$ (where n = 2 and A is the mixture of FA, MA, Cs and Rb, main peak at $2\theta = 3.12^{o}$). The corresponding XRD patterns are shown in **Figure S7.** The close peak of the pure 2D perovskite phase at $2\theta = 4.14^{o}$ compared to the additional peak from the n-OABr passivated samples at $2\theta = 4.06^{o}$ indicate that the pure 2D $(n\text{-}OA)_2Pb(I_{0.67}Br_{0.33})_4$ phase was formed on the n-OABr passivated sample. This is in agreement with a previous report showing the formation of a pure 2D perovskite phase PEA_2PbI_4 (PEA stands for phenylethylammonium) when phenylethylammonium iodide was used to passivate the perovskite surface.[16] This phase possibly came from the reaction between the n-OABr organic cation and undercoordinated Pb and halides ions at the perovskite surface. Transmission Electron Microscopy (TEM) of the cross-section of a complete perovskite solar cell passivated with n-OABr was performed, in which the passivation layer has been highlighted in yellow (**Figure 2e,f**). From the high-resolution TEM (HRTEM) of this region in **Figure 2g**, it is evident that multiple phases with very different interplanar spacing exist. One phase (in region 2 in **Figure 2g** closer to the peroskite bulk) has interplanar spacings of 6.148 Å and 3.562 Å, matching those of the (001) and (111) diffraction peaks of the 3D perovskite, respectively. The other phase (in region 1 in **Figure 2g** closer to the peroskite surface) with much larger interplanar spacing of 6.983 Å is closely related to the (012) plane of the pure 2D perovskite phase $(n\text{-}OA)_2Pb(I_{0.67}Br_{0.33})_4$ ($2\theta = 12.18^{o}$ and calculated interplanar spacing of 7.258 Å). As shown in Figure 2g, the pure 2D perovskite phase is very thin with a thickness below 20 nm. In addition, the interface between the two phases in region 1 and region 2 is not clear, indicating an inter-mixing of the two phases. Furthermore, we performed neutral impact collision ion scattering spectroscopy (NICISS) to determine the concentration depth profiles of Pb, the heaviest element present in the 3D perovskite and pure 2D perovskite phases. The presence of I, Cs and Br also influences the NICIS spectra but are more difficult to separate from Pb and the other heavy elements (I,

Cs, Br) because their atomic mass is lower than that of Pb but also have only a small difference in atomic mass.[22] As shown in **Figure 2h**, the onset of the contribution of He projectiles backscattered from Pb in the NICIS reference spectrum was 3.59. This onset value was shifted to 3.65 μs with the n-OABr passivated sample. This shift of the onset time of the Pb contribution in the spectrum to an energy loss difference of 95 ± 10 eV (**Figure 2i**). This indicates the presence of an ultrathin layer with a thickness of 16 ± 4 Å on top of the n-OABr passivated film without any Pb content (**Table S3**). It is highly possible that this ultrathin layer is the unreacted organic cation n-OABr after the passivation step. This layer is very thin and therefore it was not detected by the GIXRD measurement. Overall, the XPS, GIXRD, TEM and NICISS measurements confirm the formation of a very thin layer of pure 2D perovskite phase $(n\text{-}OA)_2Pb(I_{0.67}Br_{0.33})_4$ on top of the 3D perovskite in addition to an ultrathin layer of unreacted n-OABr organic cation after the n-OABr surface passivation.

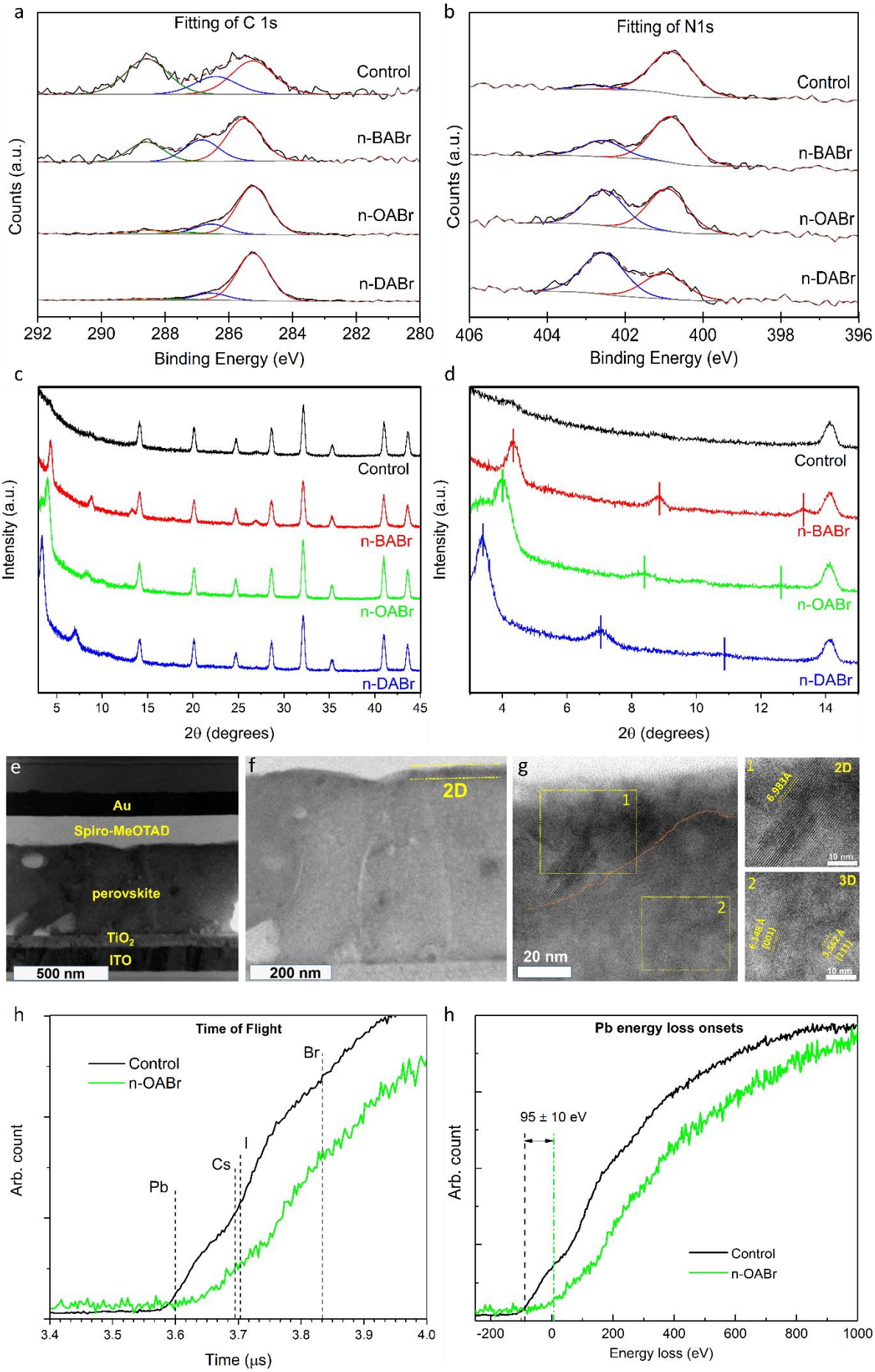
a
Fitting of C 1s
Control
n-BABr
n-OABr
n-DABr
Counts (a.u.)
292 290 288 286 284 282 280
Binding Energy (eV)
b
Fitting of N1s
Control
n-BABr
n-OABr
n-DABr
Counts (a.u.)
406 404 402 400 398 396
Binding Energy (eV)
c
Control
n-BABr
n-OABr
n-DABr
Intensity (a.u.)
5 10 15 20 25 30 35 40 45
2θ (degrees)
d
Control
n-BABr
n-OABr
n-DABr
Intensity (a.u.)
4 6 8 10 12 14
2θ (degrees)
e
Au
Spiro-MeOTAD
perovskite
TiO2
ITO
500 nm
f
2D
200 nm
g
1
2
20 nm
1
2D
6.983Å
10 nm
2
3D
6.146Å (001)
3.552Å (110)
10 nm
h
Time of Flight
Control
n-OABr
Pb
Cs
I
Br
Arb. count
3.4 3.5 3.6 3.7 3.8 3.9 4.0
Time (μs)
h
Pb energy loss onsets
95 ± 10 eV
Control
n-OABr
Arb. count
-200 0 200 400 600 800 1000
Energy loss (eV)

Figure 2. Surface elemental and phase formation study of perovskite films upon passivation. X-ray photoelectron spectra (XPS) of control and n-BABr, n-OABr and n-DABr passivated perovskite films **a** – C 1s spectrum and fitting, **b** – N 1s spectrum and fitting. **c** - XRD of control and n-BABr, n-OABr and n-DABr passivated perovskite films, **d** – XRD spectrum with 2θ from 3^{o} to 15^{o}. **e** - Cross-sectional bright-field transmission electron microscopy (BF-TEM) image of n-OABr passivated perovskite cell, **f** - low magnification BF-TEM image showing 2D/3D perovskite interface, **g** – high-resolution TEM (HRTEM) images showing the characteristic interplanar spacing of 2D and 3D perovskites. The orange line indicates the interface between the 2D and 3D perovskites. Neutral impact collision ion scattering spectroscopy (NICISS) measurements of the control (black) and n-OABr passivated (orange) perovskite films **h** - Time of Flight (TOF) and **i** – Pb energy loss onset comparison.

Effect of Passivation on Electronic Properties of Perovskite Films and Hole Extraction Efficiency in the Perovskite Solar Cells

Previous reports showed that alkylamine ligands with an amine group were capable of anchoring to the A-site of the perovskite and an ultrathin layer of densely packed ligands was formed on the perovskite surface after the treatment. [23, 24]These densely packed ligands were stabilized by van der Walls interactions, which became stronger with increasing alkyl-chain length. [25, 26] In the previous section, we identified that the ultrathin layer was indeed a 2D perovskite layer, which has been shown to be able to suppresses non-radiative recombination and act as an ion migration barrier. [27-29] Since the alkyl chain length has a strong impact on the packing density, desorption energy and carrier dynamics of ligands in this ultrathin layer,[30, 31] the alkyl chain length will also influence the passivation quality of the layer. We performed steady state photoluminescence (PL) and time resolved PL to evaluate this. As shown in **Figure 3a**, we observed significant enhancement in the PL intensity of passivated perovskite films as compared to the control perovskite film. The n-OABr passivated

film possesses the highest PL intensity, followed by the n-DABr and n-BABr passivated films. This enhancement in the PL intensity indicated the reduction in non-radiative recombination in perovskite films and was consistent with the enhancement in the V_{OC} of the passivated devices. Time-resolved PL revealed that the n-OABr passivated film also has the longest life-time, followed by the n-DABr, n-BABr passivated films and the control film (**Figure 3b**). This indicates that formation of the 2D perovskite phase on the surface of the 3D perovskite passivates the defects on the surface of the 3D perovskite. Several reports have shown that surface defects are main source of non-radiative recombination in perovskite.[32, 33] Importantly, our results show that alkylammonium organic cations with longer alkyl chain (n-OABr and n-DABr) provide better passivation effect than the one with shorter alkyl chain material (n-BABr). The results are in line with a previous report showing better passivation provided by n-OAI and n-DAI compared to n-BAI for the low bandgap $(FAPbI_3)_{0.95}(MAPbBr_3)_{0.05}$ perovskites.[11] It is worth noting that there is a slight PL peak red shift observed on all passivated perovskite films, which would require further investigation however this is beyond the scope of this work. We also captured steady state PL images of the complete devices under light and open circuit condition. As shown in **Figure 3c-f**, the n-OABr passivated device showed the highest PL counts, followed by n-DABr passivated device, n-BABr passivated device and the control device, which agreed well with the trend observed in the V_{OC} in the devices. We also performed light intensity - dependent V_{OC} measurements to examine the ideality factor (n_{id}) of perovskite solar cells passivated with different organic cations. As shown in **Figure S8** and **Table S4**, the n_{id} for the control device was found to be ~ 1.38. The n_{id} was reduced to ~1.22, ~1.13 and ~1.14 for the devices passivated with n-BABr, n-OABr and n-DABr, respectively. The reduction in the ideality factor to be closer to 1 indicates that the non-radiative recombination in the devices was suppressed when the perovskite films were passivated with large organic cation, especially by the long alkyl chain

material n-OABr and n-DABr.[34] Additionally, we performed space-charge-limit current (SCLC) measurements on the hole-only devices with a structure of glass/ITO/P3HT/perovskite/passivation layer/Spiro-MeOTAD/Au. We directly compared the control device and the device passivated with n-OABr. As shown in **Figure S9**, we found that the trap-filled limit voltage V_{TFL} in the control device was 0.166 V while the V_{TFL} in the n-OABr passivated device was 0.096 V. Since the V_{TFL} is linearly dependent on the trap density according to previous reports, [35-37] the reduction of the V_{TFL} in the passivated device indicated that trap states in perovskite films were significantly passivated by long alkyl chain organic cation at the perovskite/Spiro-MeOTAD interface. These results agree well with the photoluminescence measurements as demonstrated above.

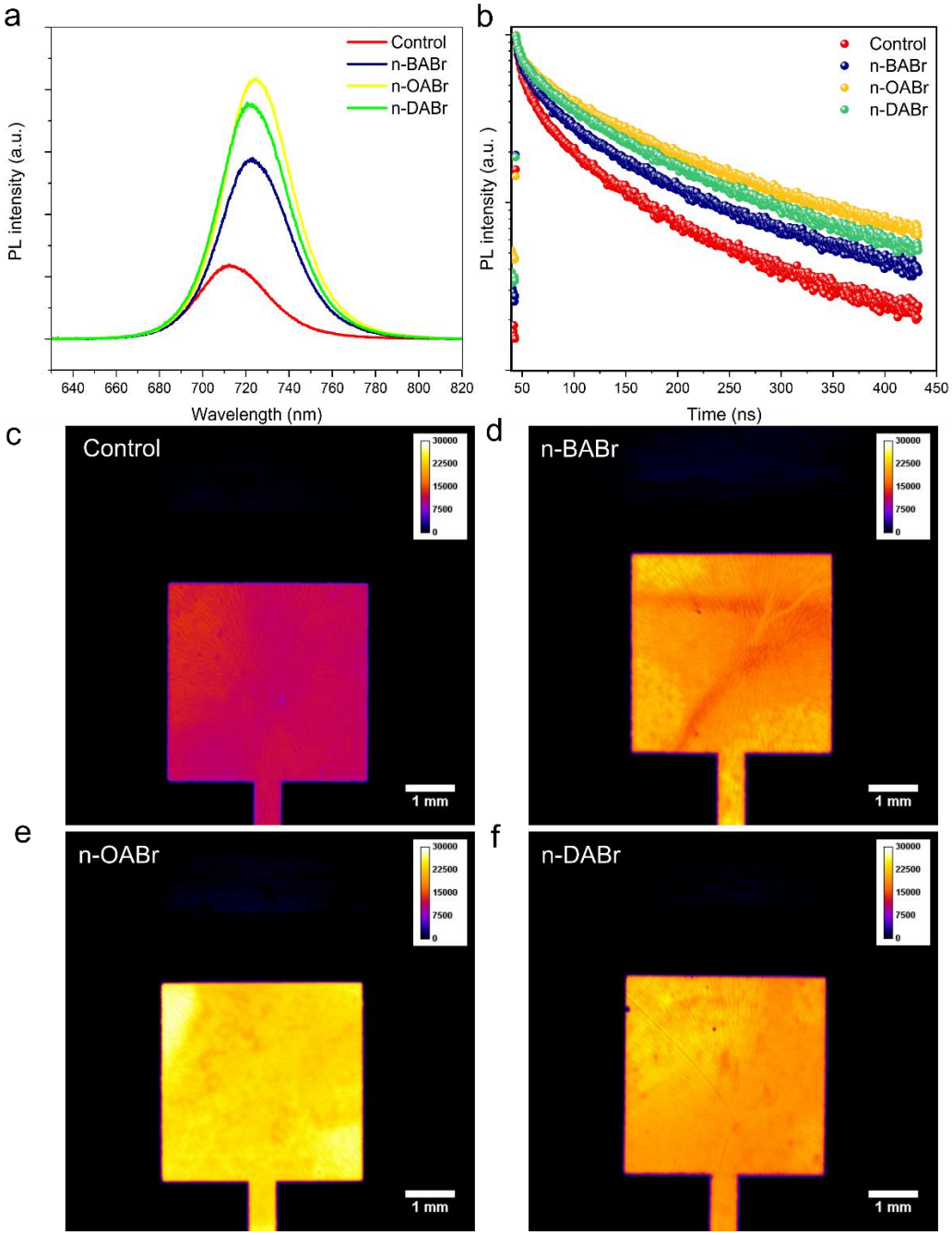

Figure 3. Photoluminescence investigation of perovskite films and perovskite solar cells upon passivation. **a** - Steady state photoluminescence (PL) spectrum and **b** - time-resolved PL of control and passivated perovskite films. **c-f** - PL images of perovskite solar cells passivated with various alkylammonium organic cations.

To elucidate how the charge carrier separation inside the perovskite solar cell changes upon passivation with long alkyl chain organic cations, we measured Electron Beam Induced Current (EBIC) profiles of the cross-sections of the control and the n-OABr passivated devices. **Figures 4a & 4b** show the SEM image and the corresponding EBIC image of a cross-section of a control device. **Figure 4c** shows the 3D surface plot of the EBIC image from **Figure 4b**. **Figures 4e to 4f** show the same set of images for a n-OABr passivated device. In the control device, we detected high EBIC signals close to the HTL and the EBIC intensity is significantly lower near to the TiO_2 electron transport layer (ETL) (**Figure 4b,c**). As the electron beam generates electron-hole pairs inside the perovskite absorber, the electrons need to travel to the ETL side, and the holes need to travel to the HTL side to be extracted to produce an electric current. The EBIC intensity indicates how efficient the charge collection is at each point inside the device.[38] The intense peaks near to the HTL indicate that electrons are extracted more efficiently than holes inside the control device. On the other hand, we observed strikingly different EBIC profiles in the passivated device. The EBIC picture and EBIC surface plot in **Figure 4e,f** show the peaks near to the ETL side instead, with the EBIC intensity near to the HTL side slightly lower. This change indicates that the hole extraction has been significantly improved in the passivated device to be equal or slightly more efficient than electron extraction. This suggests that defects on the perovskite surface acting as recombination centers for holes have been passivated by the formation of the 2D layer. In addition, the increase in the EBIC intensity inside the passivated devices may also be due to more favorable built-in electric field near to the HTL selective contacts.[39] We used ultraviolet photoelectron spectroscopy (UPS) and inverse photoemission spectroscopy (IPES) to measure the change in the electronic structure of the perovskite surface upon passivation. As shown in **Figure S10**, we observed notable reduction in the work function (WF) from 4.12 ±0.10 eV for the control film to 3.97 ±0.10 eV for the n-BABr passivated film, 3.97 ±0.10 eV for the n-OABr passivated film and

3.77 ±0.10 eV for the n-DABr passivated film. Based on the assumption that the Fermi levels align due to the equilibrium of electrons at the perovskite/HTL interface,[40] the reduction in the WF for the passivated perovskites may lead to more upward energy band bending at the interface between perovskite and Spiro-MeOTAD HTL, causing the built-in electric field to be more favorable for the hole extraction at this interface. To confirm this, we performed capacitance-voltage measurements to examine the change in the built-in voltage in the solar cell upon passivation. As shown in **Figure S11**, we found that the built-in voltage $V_{built\text{-}in}$ in the control device was 1.055 V and the $V_{built\text{-}in}$ in the n-OABr passivated device was 1.1 V. The increase in the $V_{built\text{-}in}$ in the n-OABr passivated device indicates the enhancement in the built-in electric field, which leads to the improved hole extraction in the passivated device.

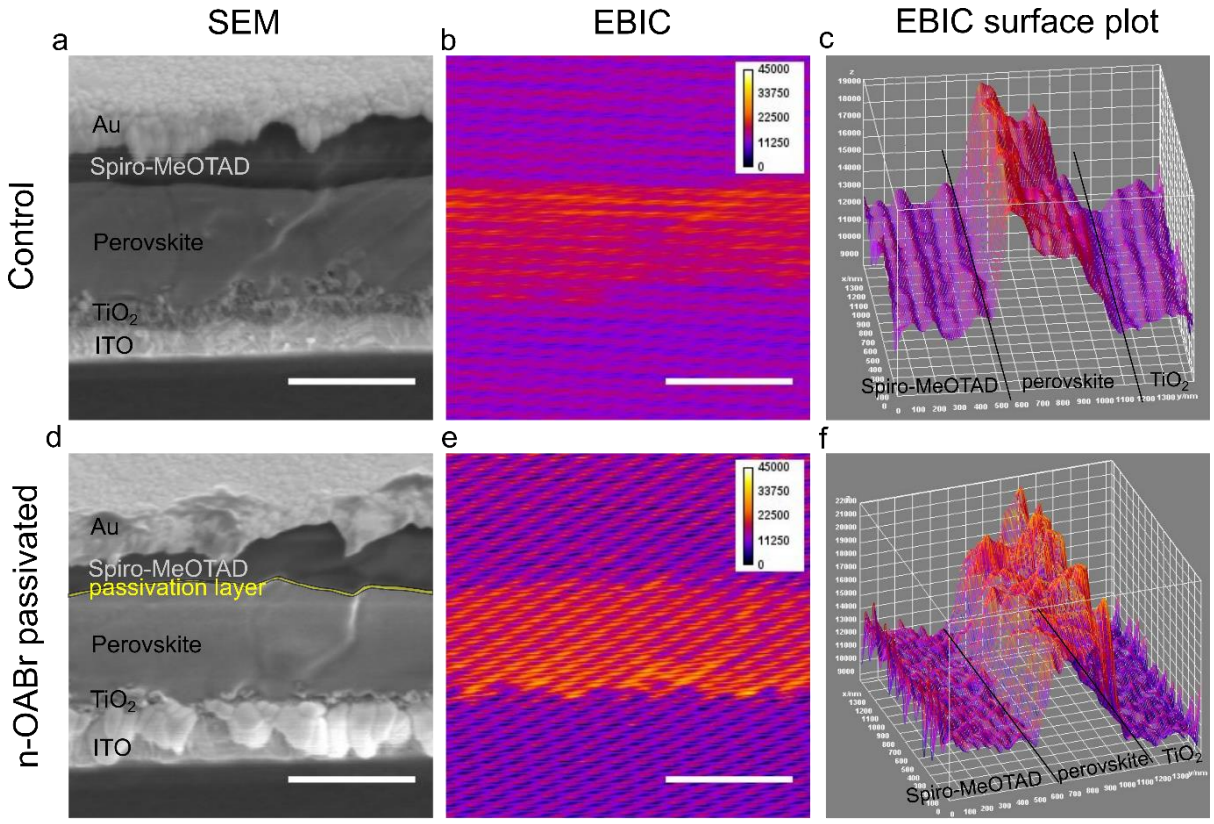

Figure 4. Electron Beam Induced Current (EBIC) measurements of perovskite solar cells. **a** – Cross-sectional SEM image, **b** – EBIC image and **c** – EBIC surface plot of control device. **d** –

Cross-sectional SEM image, **e** – EBIC image and **f**– EBIC surface plot of n-OABr passivated device.

Improvement in the Moisture Stability and Light Stability of Perovskite Solar Cells upon Passivation with Long Alkyl Chain Organic Cations

We next examined the effect of passivation on the moisture stability of the perovskite films and perovskite solar cells. We stored the perovskite films at room temperature and in a humid environment with a relative humidity (RH) ranging from 70% to 85% and measured the absorbance of the films over three weeks. As shown in **Figure 5a**, the control perovskite film degraded significantly at the outer edges as the film color changed from black to yellow after 3 weeks of storage and the absorbance spectra developed a sharp peak at ~440 nm indicating the formation of the PbI_2 phase. The inner part of the control sample degraded at a lower rate compared to the outer part of the sample, indicating that the diffusion of H_2O through the edge of the film is more significant than through the surface in the control film. The degradation in the n-BABr passivated perovskite film was very different which was more uniform across the film upon exposure to moisture (photos in **Figure 5b**). Nevertheless, the absorbance spectrum shows a substantial peak at ~ 440 nm indicating severe degradation of the n-BABr passivated film even after 1 week of storage. On the other hand, n-OABr and n-DABr passivated perovskite films are significantly more stable as the color of the perovskite films remained black even after 3 weeks of storage (photos in **Figures 5c** and **5d**). While there was still a small absorbance peak at ~440 nm in the n-DABr passivated film, the absorbance peak at ~ 450 nm in the n-OABr passivated film was negligible. It is highly possible that the formation of the ultrathin unreacted alkylammonium organic cation as the topmost layer other than the pure 2D perovskite phase was responsible for the enhancement in the moisture stability of the perovskite films passivated by long alkyl chain organic cations. When the concentration of the passivation layer was very low (less than 1 mg/ml in 2-propanol in case of n-OABr and n-DABr organic

cations), we found that the moisture stability of the perovskite film was only slightly improved. We speculate that when the concentration of the long alkyl chain organic cation passivation layer was too low, the unreacted alkylammonium organic cation layer might be too thin or might not be formed. Therefore, the enhancement in the moisture stability was not prominent upon passivation. Next, we checked the moisture stability of the control sample and found that the device degraded severely in the humid environment with the efficiency only retained 58% of the original value after 18 hours (**Figure S12**). The degradation of the control device came from both the degradation effect of the perovskite active layer and the degradation effect of the Spiro-MeOTAD HTL layer due to its hygroscopic dopants as in previous reports.[41-44] For a more meaningful investigation of the effect of various passivation treatments on the stability of perovskite solar cells, we first isolated the degradation effect coming from the Spiro-MeOTAD layer by replacing the layer with a CuPc HTL layer as in our previous report.[45] As shown in **Figure 5e**, the control device degraded severely upon exposure to moisture as the efficiency dropped to 60% of its initial performance after 144 hours. The n-BABr passivated perovskite cell had a slightly improved stability retaining 77% of its initial efficiency after the same period. On the other hand, n-OABr and n-DABr passivated devices had substantially better stability retaining 92% and 88% of their initial efficiencies, respectively. The details of all the photovoltaic parameters (V_{OC}, J_{SC}, FF and Efficiency) of the devices during the moisture exposure are shown in **Figure S13.** We also found that the contact angles of perovskite films with H_2O increased from 42.3^o for control film to 64.6^o for the n-BABr passivated film, 86^o for the n-OABr passivated film and 91.7^o for the n-DABr passivated film (**Figure S14**). Although the n-DABr passivated sample resulted in the largest contact angle with H_2O, the moisture stability of n-DABr passivated sample was slightly lower than the n-OABr passivated sample. This can be explained by the complex correlation between the surface wettability and the moisture stability of the ligand passivation layers as discussed in a recent report.[46] Zhou et

al. found that the micellization of ligands is found to greatly affect the surface ligand dissolution rate, on top of the impact from their inherent hydrophobicity. Although the n-DABr with longer chain than the n-OABr led to larger water contact angle, the aggregation-assisted ligand dissolution process in the n-DABr passivated sample could accelerate the surface degradation by its faster dissolution due to larger size micelles. Such micellization effect also depends on the nature of the underlying 3D perovskite surface with various ionic species and should be considered for the optimal design of ligand passivation layers for perovskites. We also investigated the light stability of unencapsulated perovskite solar cells with Spiro-MeOTAD HTL by keeping the devices under continuous illumination (white LED light at approximately 1 Sun intensity) and at fixed bias voltages close to their maximum power points for 80 hours. In addition, the devices were kept inside a nitrogen environment and the temperature was maintained at 25 ^{o}C during the tests. As shown in **Figure 5f**, the control device retained 85% of its original performance after operating for 80 hours. On the other hand, all the passivated devices show better irradiance stability as the devices retained between 91% and 93% of their initial efficiencies after the same period. The details of the device performance during the irradiance stability test were shown in **Figure S15**. From our previous study, light-induced phase segregation in the perovskite active layers of the devices is insignificant since the devices were kept at the voltages close to their maximum power points during the light exposure. [47] Therefore, the drop in the efficiency of perovskite solar cells was likely coming from the reversible migration of cations inside the perovskite active layers as previously reported. [48] We speculate that passivating the surface defects of the perovskite active layer reduced the negative impact of cation migration, and hence improved the light stability of the solar cells. In addition, the 2D perovskite might act as an ion migration barrier, which would also be beneficial for the light stability of perovskite cells. Furthermore, by comparing the moisture stability and light stability of the control device, it can be observed that moisture has more

negative impact than light on the device stability. Therefore, improving the moisture stability of perovskite solar cells and modules is essential for the commercialization of the technology.

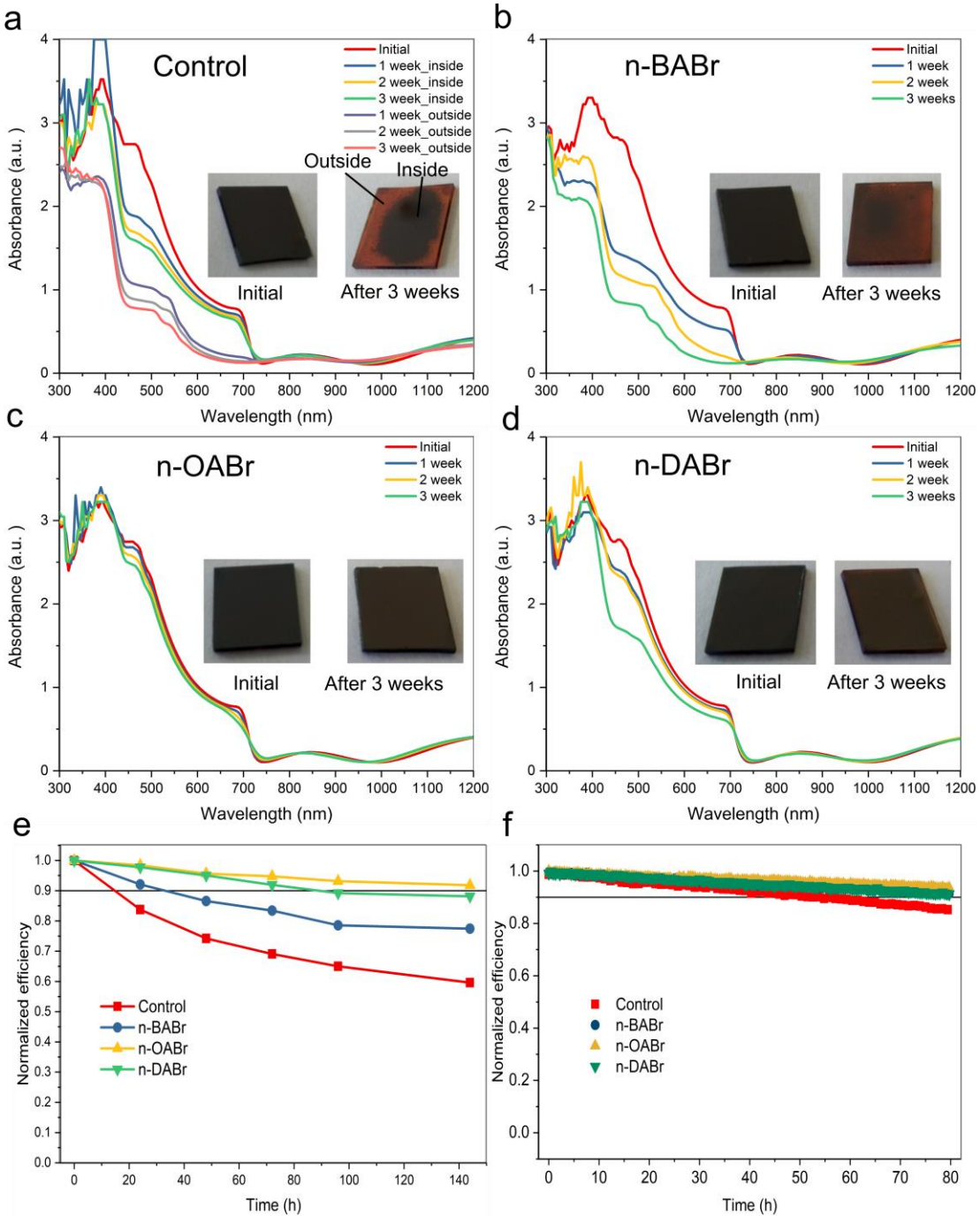

Figure 5. Examination on the moisture stability and light stability of perovskite films and perovskite solar cells. Stability of perovskite films in humid environment with the relative humidity (RH) ranging between 70% to 85% in **a** – control film, film passivated with **b** – n-BABr, **c** - n-OABr, **d** – n-DABr. **e** - Stability of unencapsulated perovskite solar cells with

CuPc HTL in the same humid environment. **f** – Stability of perovskite solar cells with Spiro-MeOTAD HTL under continuous irradiance at 1 Sun in a nitrogen environment.

Conclusions

In summary, we have demonstrated that bromide containing organic cations with long alkyl chain n-OABr and n-DABr have a greater passivation effect on 1.72 eV bandgap perovskite than the short alkyl chain n-BABr, improving the solar cell efficiency to over 19% with an open circuit voltage over 1280 mV. We showed that the reduction in perovskite surface defects and the changes in the electronic structure of the perovskite film upon passivation make it more favorable for hole extraction inside the devices. Thanks to the hydrophobic nature of the long alkyl chain organic cation, the moisture stability of perovskite solar cells was significantly enhanced as the unencapsulated device retained more than 90% of the initial efficiency after 144 hours of exposure to 70%– 85% RH. The n-OABr passivated device also showed excellent light stability, retaining 93% of the initial performance after operating for 80 hours under continuous illumination.

Author Contributions

T.D. and K.C. conceived the ideas. T.D. designed the experiment, fabricated perovskite solar cells and characterized the devices. H.P. contributed to the SEM, GIXRD and TEM measurements. Y.Y., A.K. and G.A. contributed to the XPS and UPS measurements and analysis. J.P., M.A.M., Y.W. and H.S. contributed to the optimization of perovskite solar cells. J.Z. and A.H.B. contributed to the characterization of perovskite solar cells. T.T.P. contributed to the contact angle measurements of perovskite films. T.L. and Y.L. contributed to the characterization of perovskite films. L.L. contributed to the TEM and EBIC measurements of perovskite solar cells. K.C., T.W. and K.W. supervised the research project. All the authors discussed the results and commented on the manuscript.

Conflicts of interest

There are no conflicts to declare.

Acknowledgements

This work has been supported by the Australian Government through the Australian Renewable Energy Agency (ARENA). Responsibility for the views, information or advice expressed herein is not accepted by the Australian Government. Part of the experiment was performed at Australian National Fabrication Facility (ANFF) ACT Node. T. D and J. Z. acknowledges the financial support of Postdoc Fellowships from the Australian Centre for Advanced Photovoltaics (ACAP). T. W. is the recipient of an Australian Research Council Future Fellowship (project number FT180100302) funded by the Australian Government.

References

[1] N. NREL, Best Research-Cell Efficiency Chart, in, US Department of Energy, 2021.
[2] A. Al-Ashouri, E. Köhnen, B. Li, A. Magomedov, H. Hempel, P. Caprioglio, J.A. Márquez, A.B. Morales Vilches, E. Kasparavicius, J.A. Smith, N. Phung, D. Menzel, M. Grischek, L. Kegelmann, D. Skroblin, C. Gollwitzer, T. Malinauskas, M. Jošt, G. Matič, B. Rech, R. Schlatmann, M. Topič, L. Korte, A. Abate, B. Stannowski, D. Neher, M. Stolterfoht, T. Unold, V. Getautis, S. Albrecht, Monolithic perovskite/silicon tandem solar cell with >29% efficiency by enhanced hole extraction, Science, 370 (2020) 1300-1309.
[3] D. Yang, X. Zhang, Y. Hou, K. Wang, T. Ye, J. Yoon, C. Wu, M. Sanghadasa, S. Liu, S. Priya, 28.3%-efficiency perovskite/silicon tandem solar cell by optimal transparent electrode for high efficient semitransparent top cell, Nano Energy, (2021) 105934.
[4] N.N. Lal, T.P. White, K.R. Catchpole, Optics and Light Trapping for Tandem Solar Cells on Silicon, IEEE Journal of Photovoltaics, 4 (2014) 1380-1386.
[5] J.H. Noh, S.H. Im, J.H. Heo, T.N. Mandal, S.I. Seok, Chemical Management for Colorful, Efficient, and Stable Inorganic–Organic Hybrid Nanostructured Solar Cells, Nano Letters, 13 (2013) 1764-1769.
[6] D.P. McMeekin, G. Sadoughi, W. Rehman, G.E. Eperon, M. Saliba, M.T. Hörantner, A. Haghighirad, N. Sakai, L. Korte, B. Rech, M.B. Johnston, L.M. Herz, H.J. Snaith, A mixed-cation lead mixed-halide perovskite absorber for tandem solar cells, Science, 351 (2016) 151-155.
[7] D. Kim, H.J. Jung, I.J. Park, B.W. Larson, S.P. Dunfield, C. Xiao, J. Kim, J. Tong, P. Boonmongkolras, S.G. Ji, F. Zhang, S.R. Pae, M. Kim, S.B. Kang, V. Dravid, J.J. Berry, J.Y. Kim, K. Zhu, D.H. Kim, B. Shin, Efficient, stable silicon tandem cells enabled by anion-engineered wide-bandgap perovskites, Science, 368 (2020) 155-160.
[8] T. Duong, Y. Wu, H. Shen, J. Peng, X. Fu, D. Jacobs, E.-C. Wang, T.C. Kho, K.C. Fong, M. Stocks, E. Franklin, A. Blakers, N. Zin, K. McIntosh, W. Li, Y.-B. Cheng, T.P. White, K. Weber, K. Catchpole, Rubidium Multication Perovskite with Optimized Bandgap for Perovskite-Silicon Tandem with over 26% Efficiency, Adv. Energy Mater., 7 (2017) 1700228.

[9] Y. Cho, A.M. Soufiani, J.S. Yun, J. Kim, D.S. Lee, J. Seidel, X. Deng, M.A. Green, S. Huang, A.W.Y. Ho-Baillie, Mixed 3D–2D Passivation Treatment for Mixed-Cation Lead Mixed-Halide Perovskite Solar Cells for Higher Efficiency and Better Stability, Adv. Energy Mater., 8 (2018) 1703392.
[10] Q. Jiang, Y. Zhao, X. Zhang, X. Yang, Y. Chen, Z. Chu, Q. Ye, X. Li, Z. Yin, J. You, Surface passivation of perovskite film for efficient solar cells, Nat. Photonics, 13 (2019) 460-466.
[11] H. Kim, S.-U. Lee, D.Y. Lee, M.J. Paik, H. Na, J. Lee, S.I. Seok, Optimal Interfacial Engineering with Different Length of Alkylammonium Halide for Efficient and Stable Perovskite Solar Cells, Adv. Energy Mater., 9 (2019) 1902740.
[12] T. Duong, H. Pham, T.C. Kho, P. Phang, K.C. Fong, D. Yan, Y. Yin, J. Peng, M.A. Mahmud, S. Gharibzadeh, B.A. Nejand, I.M. Hossain, M.R. Khan, N. Mozaffari, Y. Wu, H. Shen, J. Zheng, H. Mai, W. Liang, C. Samundsett, M. Stocks, K. McIntosh, G.G. Andersson, U. Lemmer, B.S. Richards, U.W. Paetzold, A. Ho-Ballie, Y. Liu, D. Macdonald, A. Blakers, J. Wong-Leung, T. White, K. Weber, K. Catchpole, High Efficiency Perovskite-Silicon Tandem Solar Cells: Effect of Surface Coating versus Bulk Incorporation of 2D Perovskite, Adv. Energy Mater., 10 (2020) 1903553.
[13] S. Gharibzadeh, B. Abdollahi Nejand, M. Jakoby, T. Abzieher, D. Hauschild, S. Moghadamzadeh, J.A. Schwenzer, P. Brenner, R. Schmager, A.A. Haghighirad, L. Weinhardt, U. Lemmer, B.S. Richards, I.A. Howard, U.W. Paetzold, Record Open-Circuit Voltage Wide-Bandgap Perovskite Solar Cells Utilizing 2D/3D Perovskite Heterostructure, Adv. Energy Mater., 9 (2019) 1803699.
[14] K.-H. Lin, A. Prlj, C. Corminboeuf, How does alkyl chain length modify the properties of triphenylamine-based hole transport materials?, Journal of Materials Chemistry C, 6 (2018) 960-965.
[15] P. Chen, Y. Bai, S. Wang, M. Lyu, J.-H. Yun, L. Wang, In Situ Growth of 2D Perovskite Capping Layer for Stable and Efficient Perovskite Solar Cells, Adv. Functional Mater., 28 (2018) 1706923.
[16] K.T. Cho, G. Grancini, Y. Lee, E. Oveisi, J. Ryu, O. Almora, M. Tschumi, P.A. Schouwink, G. Seo, S. Heo, J. Park, J. Jang, S. Paek, G. Garcia-Belmonte, M.K. Nazeeruddin, Selective growth of layered perovskites for stable and efficient photovoltaics, Energy Environ. Sci., 11 (2018) 952-959.
[17] Y. Lin, Y. Bai, Y. Fang, Z. Chen, S. Yang, X. Zheng, S. Tang, Y. Liu, J. Zhao, J. Huang, Enhanced Thermal Stability in Perovskite Solar Cells by Assembling 2D/3D Stacking Structures, J Phys Chem Lett., 9 (2018) 654-658.
[18] A.R. Milosavljević, W. Huang, S. Sadhu, S. Ptasinska, Low-Energy Electron-Induced Transformations in Organolead Halide Perovskite, Angew. Chem. Int. Ed., 55 (2016) 10083-10087.
[19] W. Huang, Y. Wang, S.K. Balakrishnan, Controllable transformation between 3D and 2D perovskites through cation exchange, Chem. Commun., 54 (2018) 7944-7947.
[20] W. Wang, H. Zhou, Y. Liu, S. Zhang, Y. Zhang, G. Wang, H. Zhang, H. Zhao, Formation of B-N-C Coordination to Stabilize the Exposed Active Nitrogen Atoms in g-C3N4 for Dramatically Enhanced Photocatalytic Ammonia Synthesis Performance, Small, 16 (2020) 1906880.
[21] Q. Zhou, L. Liang, J. Hu, B. Cao, L. Yang, T. Wu, X. Li, B. Zhang, P. Gao, High-Performance Perovskite Solar Cells with Enhanced Environmental Stability Based on a (p-FC6H4C2H4NH3)2[PbI4] Capping Layer, Adv. Energy Mater., 9 (2019) 1802595.
[22] T. Krebs, H.L. Tan, G. Andersson, H. Morgner, P. Gregory Van Patten, Increased layer interdiffusion in polyelectrolyte films upon annealing in water and aqueous salt solutions, PCCP, 8 (2006) 5462-5468.

[23] W.-Q. Wu, Z. Yang, P.N. Rudd, Y. Shao, X. Dai, H. Wei, J. Zhao, Y. Fang, Q. Wang, Y. Liu, Y. Deng, X. Xiao, Y. Feng, J. Huang, Bilateral alkylamine for suppressing charge recombination and improving stability in blade-coated perovskite solar cells, Science Advances, 5 (2019) eaav8925.
[24] S. Yang, J. Dai, Z. Yu, Y. Shao, Y. Zhou, X. Xiao, X.C. Zeng, J. Huang, Tailoring Passivation Molecular Structures for Extremely Small Open-Circuit Voltage Loss in Perovskite Solar Cells, J. Am. Chem. Soc., 141 (2019) 5781-5787.
[25] A.H. Proppe, M. Wei, B. Chen, R. Quintero-Bermudez, S.O. Kelley, E.H. Sargent, Photochemically Cross-Linked Quantum Well Ligands for 2D/3D Perovskite Photovoltaics with Improved Photovoltage and Stability, J. Am. Chem. Soc., 141 (2019) 14180-14189.
[26] X. Zheng, Y. Hou, C. Bao, J. Yin, F. Yuan, Z. Huang, K. Song, J. Liu, J. Troughton, N. Gasparini, C. Zhou, Y. Lin, D.-J. Xue, B. Chen, A.K. Johnston, N. Wei, M.N. Hedhili, M. Wei, A.Y. Alsalloum, P. Maity, B. Turedi, C. Yang, D. Baran, T.D. Anthopoulos, Y. Han, Z.-H. Lu, O.F. Mohammed, F. Gao, E.H. Sargent, O.M. Bakr, Managing grains and interfaces via ligand anchoring enables 22.3%-efficiency inverted perovskite solar cells, Nat. Energy, 5 (2020) 131-140.
[27] C. Fei, M. Zhou, J. Ogle, D.-M. Smilgies, L. Whittaker-Brooks, H. Wang, Self-assembled propylammonium cations at grain boundaries and the film surface to improve the efficiency and stability of perovskite solar cells, J. Mater. Chem. A, 7 (2019) 23739-23746.
[28] Q. Wang, Q. Dong, T. Li, A. Gruverman, J. Huang, Thin Insulating Tunneling Contacts for Efficient and Water-Resistant Perovskite Solar Cells, Adv. Mater., 28 (2016) 6734-6739.
[29] Y. Lin, Y. Bai, Y. Fang, Q. Wang, Y. Deng, J. Huang, Suppressed Ion Migration in Low-Dimensional Perovskites, ACS Energy Lett., 2 (2017) 1571-1572.
[30] X. Xiao, J. Dai, Y. Fang, J. Zhao, X. Zheng, S. Tang, P.N. Rudd, X.C. Zeng, J. Huang, Suppressed Ion Migration along the In-Plane Direction in Layered Perovskites, ACS Energy Lett., 3 (2018) 684-688.
[31] J.J. Yoo, S. Wieghold, M.C. Sponseller, M.R. Chua, S.N. Bertram, N.T.P. Hartono, J.S. Tresback, E.C. Hansen, J.-P. Correa-Baena, V. Bulović, T. Buonassisi, S.S. Shin, M.G. Bawendi, An interface stabilized perovskite solar cell with high stabilized efficiency and low voltage loss, Energy Environ. Sci., 12 (2019) 2192-2199.
[32] B. Wu, H.T. Nguyen, Z. Ku, G. Han, D. Giovanni, N. Mathews, H.J. Fan, T.C. Sum, Discerning the Surface and Bulk Recombination Kinetics of Organic–Inorganic Halide Perovskite Single Crystals, Adv. Energy Mater., 6 (2016) 1600551.
[33] H. Uratani, K. Yamashita, Charge Carrier Trapping at Surface Defects of Perovskite Solar Cell Absorbers: A First-Principles Study, J Phys Chem Lett., 8 (2017) 742-746.
[34] W. Tress, M. Yavari, K. Domanski, P. Yadav, B. Niesen, J.P. Correa Baena, A. Hagfeldt, M. Graetzel, Interpretation and evolution of open-circuit voltage, recombination, ideality factor and subgap defect states during reversible light-soaking and irreversible degradation of perovskite solar cells, Energy Environ. Sci., 11 (2018) 151-165.
[35] M. Zhang, M. Ye, W. Wang, C. Ma, S. Wang, Q. Liu, T. Lian, J. Huang, Z. Lin, Synergistic Cascade Carrier Extraction via Dual Interfacial Positioning of Ambipolar Black Phosphorene for High-Efficiency Perovskite Solar Cells, Adv. Mater., 32 (2020) 2000999.
[36] B. Wang, H. Li, Q. Dai, M. Zhang, Z. Zou, J.-L. Brédas, Z. Lin, Robust Molecular Dipole-Enabled Defect Passivation and Control of Energy-Level Alignment for High-Efficiency Perovskite Solar Cells, Angew. Chem. Int. Ed., 60 (2021) 17664-17670.
[37] M. Zhang, X. Cui, Y. Wang, B. Wang, M. Ye, W. Wang, C. Ma, Z. Lin, Simple route to interconnected, hierarchically structured, porous Zn2SnO4 nanospheres as electron transport layer for efficient perovskite solar cells, Nano Energy, 71 (2020) 104620.

[38] E. Edri, S. Kirmayer, S. Mukhopadhyay, K. Gartsman, G. Hodes, D. Cahen, Elucidating the charge carrier separation and working mechanism of CH3NH3PbI3−xClx perovskite solar cells, Nat. Commun., 5 (2014) 3461.
[39] E. Edri, S. Kirmayer, A. Henning, S. Mukhopadhyay, K. Gartsman, Y. Rosenwaks, G. Hodes, D. Cahen, Why Lead Methylammonium Tri-Iodide Perovskite-Based Solar Cells Require a Mesoporous Electron Transporting Scaffold (but Not Necessarily a Hole Conductor), Nano Letters, 14 (2014) 1000-1004.
[40] Y. Yin, A. Sibley, J.S. Quinton, D.A. Lewis, G.G. Andersson, Dipole Formation at the MoO3/Conjugated Polymer Interface, Adv. Functional Mater., 28 (2018).
[41] H.-S. Kim, J.-Y. Seo, N.-G. Park, Impact of Selective Contacts on Long-Term Stability of CH3NH3PbI3 Perovskite Solar Cells, The Journal of Physical Chemistry C, 120 (2016) 27840-27848.
[42] L. Zheng, Y.-H. Chung, Y. Ma, L. Zhang, L. Xiao, Z. Chen, S. Wang, B. Qu, Q. Gong, A hydrophobic hole transporting oligothiophene for planar perovskite solar cells with improved stability, Chem. Commun., 50 (2014) 11196-11199.
[43] T.A. Berhe, W.-N. Su, C.-H. Chen, C.-J. Pan, J.-H. Cheng, H.-M. Chen, M.-C. Tsai, L.-Y. Chen, A.A. Dubale, B.-J. Hwang, Organometal halide perovskite solar cells: degradation and stability, Energy Environ. Sci., 9 (2016) 323-356.
[44] J. Xu, O. Voznyy, R. Comin, X. Gong, G. Walters, M. Liu, P. Kanjanaboos, X. Lan, E.H. Sargent, Crosslinked Remote-Doped Hole-Extracting Contacts Enhance Stability under Accelerated Lifetime Testing in Perovskite Solar Cells, Adv. Mater., 28 (2016) 2807-2815.
[45] T. Duong, J. Peng, D. Walter, J. Xiang, H. Shen, D. Chugh, M. Lockrey, D. Zhong, J. Li, K. Weber, T.P. White, K.R. Catchpole, Perovskite Solar Cells Employing Copper Phthalocyanine Hole-Transport Material with an Efficiency over 20% and Excellent Thermal Stability, ACS Energy Lett., 3 (2018) 2441-2448.
[46] H. Zhou, J. Wang, M. Wang, S. Lin, Competing Dissolution Pathways and Ligand Passivation-Enhanced Interfacial Stability of Hybrid Perovskites with Liquid Water, ACS Appl. Mater. Interfaces, 12 (2020) 23584-23594.
[47] T. Duong, H.K. Mulmudi, Y. Wu, X. Fu, H. Shen, J. Peng, N. Wu, H.T. Nguyen, D. Macdonald, M. Lockrey, T.P. White, K. Weber, K. Catchpole, Light and Electrically Induced Phase Segregation and Its Impact on the Stability of Quadruple Cation High Bandgap Perovskite Solar Cells, ACS Appl. Mater. Interfaces, 9 (2017) 26859-26866.
[48] K. Domanski, B. Roose, T. Matsui, M. Saliba, S.-H. Turren-Cruz, J.-P. Correa-Baena, C.R. Carmona, G. Richardson, J.M. Foster, F. De Angelis, J.M. Ball, A. Petrozza, N. Mine, M.K. Nazeeruddin, W. Tress, M. Grätzel, U. Steiner, A. Hagfeldt, A. Abate, Migration of cations induces reversible performance losses over day/night cycling in perovskite solar cells, Energy Environ. Sci., 10 (2017) 604-613.